

“Cold” diapirs triggered by intrusion of the Bushveld Complex: Insight from two-dimensional numerical modeling

Taras V. Gerya*

Geological Institute, Swiss Federal Institute of Technology Zurich, CH 8092 Zurich, Switzerland, and Institute of Experimental Mineralogy, Russian Academy of Sciences, Chernogolovka, Moscow District 142432, Russia

Ronald Uken

Juergen Reinhardt

Michael K. Watkeys

School of Geological and Computer Science, University of Natal, 4041 Durban, South Africa

Walter V. Maresch

Institute of Geology, Mineralogy and Geophysics, Ruhr-University Bochum, 44780 Bochum, Germany

Brendan M. Clarke

Council for Geoscience, P.O. Box 900, 3200 Pietermaritzburg, South Africa

ABSTRACT

Diapir and dome structures on a scale of meters to kilometers are widespread in Earth’s continental crust and represent an important tectonic element of cratons, orogenic belts, and sedimentary basins. These structures advect heat from lower to higher crustal levels, often producing pronounced prograde contact metamorphic aureoles. This standard thermal situation is violated by the up to 8 km in diameter migmatitic domes and diapirs of metasedimentary rocks that penetrate the world’s largest layered intrusion, the Bushveld Complex. These domes and diapirs rose with an average rate of about 8 mm/yr and were characterized by an unusual inverted thermal structure, with the cores of the structures 200–300 °C colder than the rims. Numerical modeling supports the interpretation that the process was triggered by the emplacement of an 8-km-thick, hot, dense mafic magma over a cold, less dense sedimentary succession, resulting in a dramatic lowering of the viscosity of the sediments during contact metamorphism and partial melting. Dome and diapir nucleation is interpreted to have been defined by the formation of initial anticline-shaped disturbances related to fingered lateral injection of the Lower Zone of the Bushveld intrusion between the felsic roof and sedimentary floor sequence. The partially molten, mobile, but *relatively cold* domes and diapirs promoted cooling of the giant magma chamber, rapidly bringing cooler material into higher crustal levels, and freezing the surrounding magmas. We argue that our work has a more general significance as similar thermal structures should be a widespread feature associated with partially molten mantle diapirs (“cold plumes”) generated in the proximity of subducting slabs. These structures are likely responsible for rapid upward melt transport above subduction zones and for the associated volcanic activity. The exposed structures

*Taras.Gerya@erdw.ethz.ch

observed in the Bushveld Complex provide a unique opportunity to study the “cold” diapir/plume phenomenon, thus leading to a broader recognition and understanding of this geological process.

Keywords: diapirism, domes, numerical modeling, Bushveld Complex, partial melting, subduction zones.

INTRODUCTION

Diapirs and domes on a scale of meters to kilometers are widespread in Earth’s continental crust (Ramberg, 1981) and represent an important tectonic element of cratons, orogenic belts, and sedimentary basins. These structures advect heat from lower to higher crustal levels, often producing pronounced prograde contact metamorphic aureoles. Consequently, the existence of a positive thermal anomaly (e.g., Bittner and Schmeling, 1995; Gerya et al., 2000) within such a rising structure is the thermal norm. We use two-dimensional coupled thermomechanical numerical modeling to show that migmatitic diapirs of metasedimentary rocks found in the Bushveld Complex (Uken and Watkeys, 1997) were characterized by a 200–300 °C negative thermal anomaly at the time of ascent (Gerya et al., 2003). Furthermore, we argue that similar inverted thermal structures should be a widespread feature associated with partially molten mantle diapirs generated in the proximity of subducting slabs.

GEOLOGICAL SETTING

The emplacement of the 2061 ± 27 Ma (Walraven et al., 1990) ultramafic and mafic magmas of the Rustenburg Layered Suite into the Early Proterozoic Transvaal Supergroup occurred as multiple magma injections along the contact between the Pretoria Group and the overlying Rooiberg Group (Fig. 1), both of which are about 5 km in thickness (Eriksson et al., 1993; Hutton and Schweitzer, 1995). The Rustenburg Layered Suite now consists of a sill-shaped sequence of mafic-ultramafic rocks up to 8 km thick (Du Plessis and Kleywegt, 1987; Cawthorn et al., 1998). Simultaneous isostatic subsidence of the intrusion produced the present regional, basin-shaped lopolithic geometry. The Rustenburg Layered Suite is subdivided, from bottom to top, into the Marginal, Lower, Critical, Main, and Upper Zones (Cameron, 1978, 1980, 1982; Von Gruenewaldt et al., 1985) (Fig. 1B). The relatively thin Marginal Zone comprises a diverse assemblage of fine-grained norites and pyroxenites. The Lower Zone forms discrete separated magma compartments, each consisting of alternating bronzitite, harzburgite, and dunite (Sharpe, 1986). The Critical Zone oversteps the Lower Zone and consists mainly of norites, leuconorites, and anorthosites, which contain economically important chromite and platinumiferous horizons. The Main Zone forms a thick succession of dominantly gabbroic composition, followed by the Upper Zone, comprised of ferrogabbros with cumulus magnetite layers. The floor of the Rustenburg Layered Suite consists of contact-metamorphosed Pretoria Group shales and sandstones with minor carbonates and

volcaniclastics. These overlie dolomite and banded ironstones of the Chuniespoort Group that are relatively unaffected by metamorphism and associated deformation.

The volcanic Rooiberg Group that forms the roof to the Rustenburg Layered Suite is dominated by felsic volcanics and volcaniclastics. The upper units of the Rooiberg Group are considered contemporaneous with the intrusion of the Rustenburg

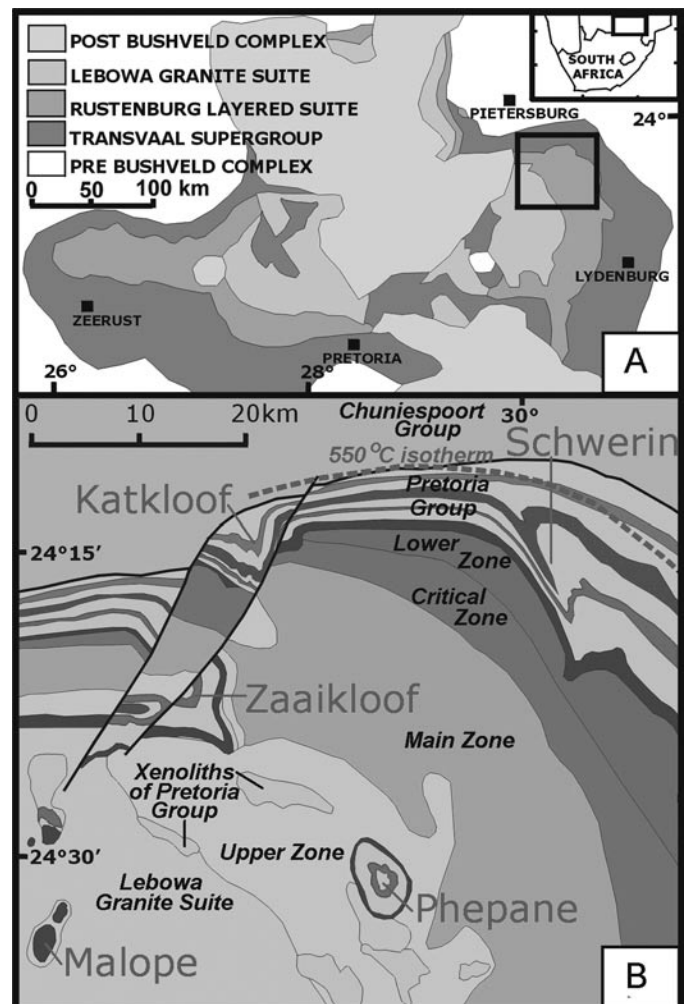


Figure 1. Geological position of domes and diapirs in the Bushveld Complex, South Africa. A. The Bushveld Complex showing the diapir field of the northeast. B. Geology of the diapiric area showing the distribution and names of the main diapiric structures. A color version of this figure is on the CD-ROM accompanying this volume.

Layered Suite (Hatton and Schweitzer, 1995) and were intruded by the Lebowa Granite Suite. Precise sensitive high-resolution ion microprobe (SHRIMP) ages for the crystallization of the Rooiberg Group, Rustenburg Layered Suite, and Lebowa Granite Suite are statistically indistinguishable, indicating that all magmatic activity occurred within the attainable precision of 3–5 m.y. (Harmer and Armstrong, 2000).

The emplacement of the Rustenburg Layered Suite produced a considerable contact-metamorphic aureole in the floor. Regionally, the aureole thickens from the south in the Pretoria area, where it is poorly developed, toward the east, west, and north (Fig. 1). The peak average thermal gradient across the aureole was 80 ± 20 °C/km, and pressures were between 2.1 ± 0.4 kbar in the upper part of the Pretoria Group and 2.4 ± 0.9 kbar in the lower part of the Pretoria Group (Kaneko and Miyano, 1990). The metamorphic zonation in the argillaceous floor rocks of the Pretoria Group of the Transvaal Supergroup is characterized in the lower and outermost part of the aureole by assemblages with chloritoid and biotite, followed by a wide andalusite zone in which chistalitic andalusite is found in association with chloritoid, staurolite, garnet, and cordierite. These rocks pass up-grade into a fibrolite zone, in which fibrolite coexists with andalusite, followed by K-feldspar produced by muscovite + quartz breakdown. The innermost part of the aureole is characterized by partial melting and extensive migmatite development (Kaneko and Miyano, 1990; Uken, 1998; Waters and Lovegrove, 2002; Johnson et al., 2003; Harris et al., 2003).

DOMAL AND DIAPIRIC STRUCTURES

On a regional scale, the emplacement of the Bushveld Complex magmas into the Kaapvaal Craton was facilitated by a combination of craton-wide lateral extension that accompanied plume-related magmatic underplating and gravitational loading (Uken, 1998). Isostatic adjustment in response to subsidence of the Rustenburg Layered Suite (forming the present, lopolithic basin shape) probably resulted in the uplift of three groups of periclinal-shaped domal structures that developed in response to magmatic loading:

1. Large basement domes (~100 km in diameter) around the perimeter of the Bushveld Complex;
2. Medium sized domes (~40 km in diameter) within the complex that extend to the base of the Transvaal Supergroup;
3. Small-scale domes and diapirs (~8km in diameter) that occur only within the contact-metamorphosed Pretoria Group floor of the Transvaal Supergroup (Uken and Watkeys, 1997; Uken, 1998).

Small-scale domal floor structures are developed in the northeastern Bushveld Complex where the contact aureole penetrates the floor rocks to a depth of almost 5 km. The occurrence of deformed Transvaal Supergroup country rocks within the Bushveld Complex has been attributed to a number of mechanisms, including pre-intrusive folding and doming, syn-intrusive xenolith development or doming, and post-intrusive thrusting

(Hartzer, 1995, and references therein). Sharpe and Chadwick (1982), for example, reinterpreted the structures to have resulted from folding produced by the emplacement of the Rustenburg Layered Suite into a subsiding compressional basin (Sharpe and Snyman, 1980). Button (1978) was the first to suggest a diapiric origin for the northeastern Bushveld Complex structures due to the buoyant ascent of Transvaal Supergroup floor rocks into the overlying ultramafic and mafic magmas of the Bushveld Complex. This idea has recently been supported by detailed structural-geological work by Uken and Watkeys (1997).

At least seven large diapiric structures of contact-metamorphosed Pretoria Group rocks penetrate the overlying Rustenburg Layered Suite (Uken and Watkeys, 1997; Uken, 1998), of which the Katkloof, Schwerin, Zaaikloof, Malope, and Phepane are the best developed (Figs. 1B and 2A). Geophysical evidence confirms that the Malope structure (Marlow and Van der Merwe, 1977) and the Phepane structure (Molyneux and Klinkert, 1978) (Fig. 2A) are not large xenoliths, but are attached to the floor of the Rustenburg Layered Suite in the same way as the diapiric structures along the Suite perimeter, where their nature is clearly seen. These structures are cut by a different erosional section, enabling reconstruction of the original diapir geometry and internal structure (Uken and Watkeys, 1997) (Fig. 2A). Diapir formation is restricted to rocks above a décollement zone that developed along zones of lithological competency contrast and corresponds approximately with the 550 °C peak metamorphic isotherm (Uken and Watkeys, 1997). This décollement zone lies between 3.8 km and 2.3 km below the Rustenburg Layered Suite contact (Uken and Watkeys, 1997). Domes and diapirs are irregularly spaced, with an average separation between diapirs of ~30 km (Fig. 1B). The wavelength varies from 22 km for the western domes to 44 km between the Phepane and Steelpoort domes (Fig. 1B). Diapir and dome geometries range between gentle, open folds to tighter, asymmetric, cusped-like fold profiles (Katkloof, Schwerin, Zaaikloof). The asymmetrical bulbous shape of the Phepane pericline has a classic diapiric geometry, with overturned and overhanging margins (Fig. 2A). The Malope structure represents a shallow-dipping dome head with limbs dipping at an average of 30° (Marlow and Van der Merwe, 1977). Strongly lineated, boudinaged, and foliated rocks are developed between the diapirs, with fabrics consistent with extreme loading and near-bedding-parallel extension with flow toward the diapir culminations (Uken and Watkeys, 1997). The maximum elevation difference between the domes and interdomal areas is ~6.5 km, implying that the diapirs rose to as much as ~10 km above their décollement zone (Uken and Watkeys, 1997). Ponding of Lower Zone magmas in the Rustenburg Layered Suite, truncation of Upper Zone magmatic layers, and thinning and draping of magmatic sections above the diapirs indicate that the diapirs were initiated in the early stages of emplacement of the Rustenburg Layered Suite magmas and continued to rise as the magma chamber thickened. Furthermore, the diapirs are causally related to initial perturbations in the magma chamber floor that resulted from lobate lateral advancement of Lower Zone magmas (Uken

and Watkeys, 1997). Backstripping of the Rustenburg Layered Suite in the northeastern Bushveld Complex shows that the emplacement of Lower Zone magmas was initiated as a series of isolated finger-shaped intrusions separated by interfingered areas (Uken and Watkeys, 1997). According to this model, folds were developed between adjacent intrusion fingers, which remained as cusp-shaped folds once the fingers had mostly coalesced into a single sheet (Fig. 2B). During the emplacement of the Lower

Zone magmas, deformation of the interfinger zone provided suitable floor perturbations, which formed the loci to subsequent floor diapirism with further magma additions and increased floor ductility.

MODEL DESIGN AND NUMERICAL IMPLEMENTATION

Initial and Boundary Conditions

The development of diapirs of partially molten crustal material related to the magmatic underplating of felsic continental crust by large amounts of mafic magma was studied numerically by Bittner and Schmeling (1995). In their model, heating of the (source) crustal sequence occurs from below, initiating upward-directed propagation of a melting front and triggering crustal diapirism driven by a density contrast between underlying partially molten and overlying solid crustal rocks. In the Bushveld Complex, however, the situation is reversed: the heating of the (source) sedimentary sequence occurred from above, the melting front propagated downward, and diapirism was driven by a density contrast between the crystallizing hot and heavy mafic intrusion and the underlying, less dense metamorphosed and partially molten sedimentary rocks.

Adopting the approach of Bittner and Schmeling (1995), we designed a two-dimensional numerical model (Fig. 3) based on the three-dimensional conceptual model of Uken and Watkeys (1997) (Fig. 2B). The initial and boundary conditions and other relevant parameters, such as the lithologic stratification and initial isotherm distribution, are displayed in Figure 3. The high (200–300 kg/m³) density contrast between heavy mafic magma and less dense sedimentary rocks creates favorable conditions for the development of compositionally driven Rayleigh-Taylor instability along the floor of the Rustenburg Layered Suite intrusion. To ensure smooth continuity of the evolving non-steady-state temperature field across the lower boundary of the truncated regional model, we have used the infinity-like boundary condition $\partial^2 T / \partial z^2 = 0$ (Turcotte and Schubert, 1973; Gerya et al., 2002), where T is temperature in Kelvin and z is the vertical coordinate.

The internal geometry of the model depicted in Figure 3 is based on the geological, geochronological, and stratigraphic data for the northeastern Bushveld Complex discussed above. The physical properties of the rocks are listed in Table 1. Taking into account the average distance between diapirs, we used a 30 km characteristic lateral box size. Nucleation of a diapir is related to the presence of an initial anticline of small amplitude on the intrusion floor in the central portion of the model. The formation of similar anticlines can logically be related to the fingered or segmented injection of the Lower Zone of the Rustenburg Layered Suite at the initial stage of emplacement of the mafic intrusion (Fig. 2B). The sensitivity of the model with respect to the height of the initial anticline, the lateral box size (initial wavelength), and the initial thermal structure has also been investigated (Table 2).

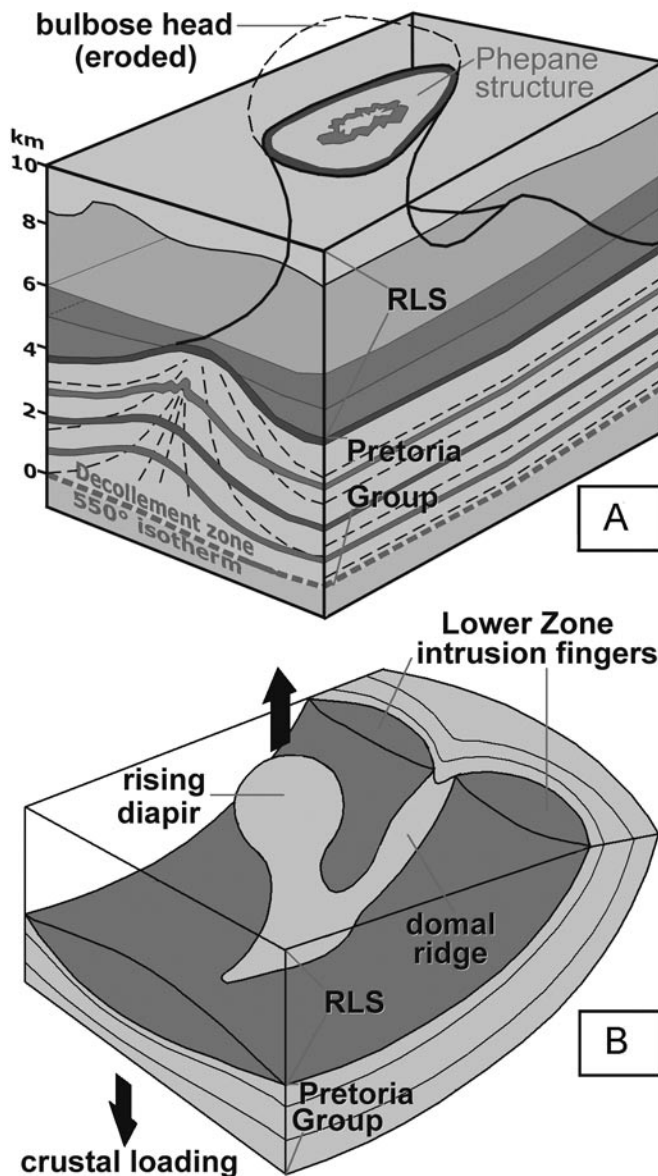


Figure 2. Idealized three-dimensional geometry and structure of the Phepane diapir (A), and three-dimensional conceptual model of development of domes and diapirs in the Bushveld Complex (B) (Uken and Watkeys, 1997). Dashed lines in A show foliation trace. A color version of this figure is on the CD-ROM accompanying this volume.

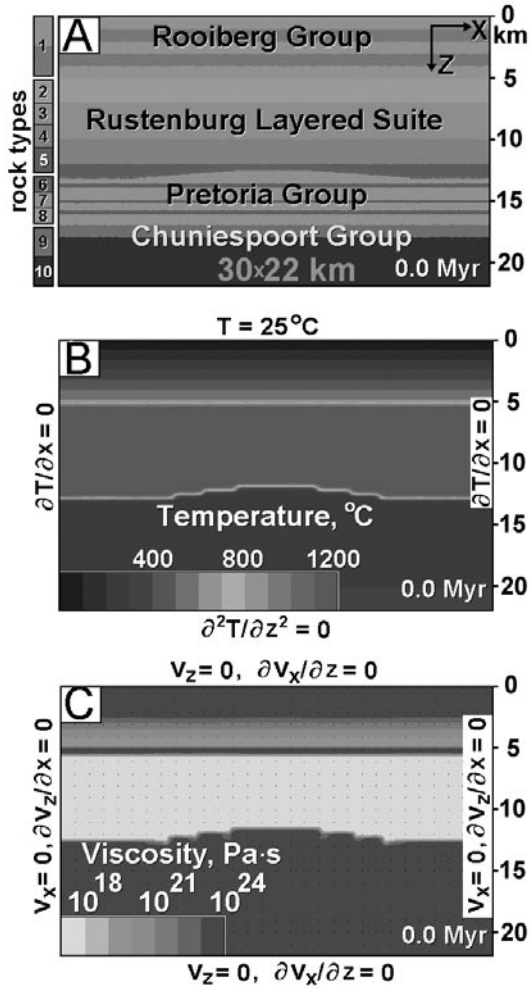


Figure 3. Design, initial, and boundary conditions of two-dimensional numerical experiments. The grid configuration is 91×67 regularly spaced points; 148,500 markers are employed. A. Initial lithological structure of the model consisting of 10 major rock types (Uken and Watkeys, 1997) (see numbering top to bottom): Rooiberg Group (5 km thickness) 1—felsic volcanics and Lebowa granites; Rustenburg Layered Suite (8 km thickness) 2—Upper Zone, 3—Main Zone, 4—Critical Zone, 5—Lower Zone; Pretoria Group (4 km thickness) 6—quartzites, 7—pelitic rocks, 8—diabases; Chuniespoort Group (>4 km thickness) 9—banded iron formations, 10—siliceous dolomites. B. Initial temperature structure of the model and thermal boundary conditions. C. Initial viscosity structure of the model and mechanical boundary conditions. A color version of this figure is on the CD-ROM accompanying this volume.

TABLE 1. MATERIAL PROPERTIES* USED IN 2-D NUMERICAL EXPERIMENTS

Units	Rock type	Cp J/(K kg)	ρ_0 kg/m ³	k W/(m K)	Flow law (solid rocks)	T_{solidus} (K)	T_{liquidus} (K)	H_L (kJ/kg)	H_f 10 ⁻⁶ W/m ³
Rooiberg Group	Felsic volcanics and Lebowa granites	1000	2700 (solid) 2400 (molten)	2.5	wet granite	675	925	300	2
RLS	Mafic/ultramafic rocks of the Upper, Main, Critical and Lower Zones	1000	3000 (solid) 2900 (molten)	3.5	plagioclase (An ₇₅)	950	1100	380	0.25
Pretoria Group	Quartzites	1000	2650 (solid) 2450 (molten)	2.5	wet quartzite	675	925	300	1
	Pelitic rocks	1000	2600 (solid) 2400 (molten)	2.5	wet granite	675	925	300	2
	Diabases	1000	3000	3.5	plagioclase (An ₇₅)	—	—	—	0.25
Chuniespoort Group	Banded iron formations	1000	3000	2.5	wet quartzite	—	—	—	0.5
	Siliceous dolomites	1000	2500	2.5	wet quartzite	—	—	—	0.25

Note: Cp—heat capacity; H_L —latent heat of melting; k— thermal conductivity; RLS—Rustenburg Layered Suite; T_{solidus} and T_{liquidus} —solidus and liquidus temperature, respectively; ρ_0 — density.

*From Bittner and Schmeling (1995), Turcotte and Schubert (1982), and Ranalli (1995).

TABLE 2. PARAMETERS OF NUMERICAL MODELS STUDIED

Number	Figure	Rheology	Lateral width (km)	Height of the initial anticline (m)	Initial $\partial T/\partial z$ within the Rooiberg Group, ($^{\circ}\text{C}/\text{km}$)	Initial T of the RLS ($^{\circ}\text{C}$)	Final height of the diapir (km)	Final shape of the diapir
1 (ront1)	3, 4	standard	30	1000	120 (25–625 $^{\circ}\text{C}$)	1200	11.3	finger-like
2 (ronw1)	5a	standard	30	800	120 (25–625 $^{\circ}\text{C}$)	1200	4.1	dome-like
3 (ronx1)	5b	standard	30	1200	120 (25–625 $^{\circ}\text{C}$)	1200	9.7	mushroom-like
4 (ronanew1)	5c	standard	30	1000	40 (25–225 $^{\circ}\text{C}$)	1200	2.5	dome-like
5 (ronbnew1)	5d	standard	30	1000	200 (25–1025 $^{\circ}\text{C}$)	1200	13.3	mushroom-like
6 (roncnew1)	5e	standard	30	1000	120 (25–625 $^{\circ}\text{C}$)	1100	1.6	dome-like
7 (rondnew1)	5f	standard	30	1000	120 (25–625 $^{\circ}\text{C}$)	1300	14.2	mushroom-like
8 (ronhnew1)	6a	strong RLS*	30	1000	120 (25–625 $^{\circ}\text{C}$)	1200	1.6	dome-like
9 (rongnew1)	6b	weak RLS*	30	1000	120 (25–625 $^{\circ}\text{C}$)	1200	13.8	mushroom-like
10 (ronjnew1)	6c	strong Transvaal Sgr.*	30	1000	120 (25–625 $^{\circ}\text{C}$)	1200	2.0	dome-like
11 (roninew1)	6d	weak Transvaal Sgr.*	30	1000	120 (25–625 $^{\circ}\text{C}$)	1200	15.8	mushroom-like
12 (ronz1)	6e	standard	20	1000	120 (25–625 $^{\circ}\text{C}$)	1200	7.8	dome-like
13 (rony1)	6f	standard	60	1000	120 (25–625 $^{\circ}\text{C}$)	1200	12.9	finger-like
14 (ronenew1)	–	standard	30	1000	40 (25–225 $^{\circ}\text{C}$)	1300	9.2	mushroom-like
15 (ronfnew1)	–	standard	30	1000	100 (25–525 $^{\circ}\text{C}$)	1200	5.7	dome-like
16 (ronu1)	–	standard	30	500	120 (25–625 $^{\circ}\text{C}$)	1200	0.8	dome-like
17 (ronv1)	–	standard	30	1500	120 (25–625 $^{\circ}\text{C}$)	1200	10.3	mushroom-like

Note: RLS—Rustenburg Layered Suite; Sgr—Supergroup.

*strong/weak rheology is implemented by decreasing/increasing the A_D value in Eq. 4 by a factor of 10.

Melting and Crystallization Model

To model the changes in the physical properties of rocks (Table 1) arising from partial melting and crystallization, we have adopted the algorithm developed by Bittner and Schmeling (1995) for modeling magmatic underplating. According to this model, melting and crystallization of metasedimentary and magmatic rocks is temperature-dependent and occurs in the T -region between the wet solidus and dry liquidus. As a first approximation, the degree of melting is taken to increase linearly with the temperature according to the relations

$$M = 0 \text{ at } T < T_{\text{solidus}}, \quad (1a)$$

$$M = \frac{(T - T_{\text{solidus}})/(T_{\text{liquidus}} - T_{\text{solidus}})}{T_{\text{solidus}} < T < T_{\text{liquidus}}} \text{ at} \quad (1b)$$

$$M = 1 \text{ at } T > T_{\text{liquidus}}, \quad (1c)$$

where M is the volumetric fraction of melt at a temperature T ; T_{solidus} and T_{liquidus} are, respectively, solidus and liquidus temperature given in Table 1 for the different rock types.

An effective density, ρ_{eff} of partially molten rocks is calculated from the formula

$$\rho_{\text{eff}} = \rho_{\text{solid}} - M(\rho_{\text{solid}} - \rho_{\text{molten}}), \quad (2)$$

where ρ_{solid} and ρ_{molten} are, respectively, densities of solid and molten rock (Table 1).

The effects of latent heat are accounted for by an increased effective heat capacity of partially molten rock (Cp_{eff}) calculated according to the equation

$$Cp_{\text{eff}} = Cp + H_L/(T_{\text{liquidus}} - T_{\text{solidus}}), \quad (3)$$

where Cp is the heat capacity in $\text{J}/(\text{K kg})$ and H_L is the latent heat of melting of the lithological unit in J/kg .

The Rheological Model

Following Bittner and Schmeling (1995), the stress- and temperature-dependent creep viscosity for solid rocks (i.e., $M < 0.1$) is defined in terms of deformation invariants by (Ranalli, 1995)

$$\eta = (\dot{\epsilon}_{\text{II}})^{(1-n)/2n} F(A_D)^{-1/n} \exp(E/nRT), \quad (4)$$

where $\dot{\epsilon}_{\text{II}} = 1/2 \dot{\epsilon}_{ij} \cdot \dot{\epsilon}_{ij}$ is the second invariant of the strain rate tensor, with dimension s^{-2} ; η is the creep viscosity, Pa s ; F is a dimensionless coefficient depending on the type of experiments on which the flow law is based (e.g., $F = 2^{(1-n)/n}/3^{(1+n)/2n}$ for triaxial compression and $F = 2^{(1-2n)/n}$ for simple shear).

The rheology of the mafic rocks is taken to be represented by a flow law for dislocation creep of plagioclase with composition An_{75} , with $E = 238 \text{ kJ} \cdot \text{mol}^{-1}$, $n = 3.2$, and $\log A_D = -3.5$ (A_D given in $\text{MPa}^{-n} \cdot \text{s}^{-1}$), as quoted in Ranalli (1995).

We have used flow laws for wet felsic geomaterials to represent the rheology of metasediments and the granitic rocks of the Transvaal Supergroup. These take into account both the

felsic composition of these rocks and the presence of fluid during contact metamorphism and partial melting (Kaneko and Miyano, 1990; Uken, 1998; Waters and Lovegrove, 2002; Johnson et al., 2003; Harris et al., 2003). The rheology of metapelites and granites is modeled by a flow law for dislocation creep of wet granite, with $E = 137 \text{ kJ}\cdot\text{mol}^{-1}$, $n = 1.9$, and $\log A_D = -3.7$ (Ranalli, 1995). The rheology of the quartzites, banded iron formations, and siliceous dolomites is modeled by a flow law for dislocation creep of wet quartzite, with $E = 154 \text{ kJ}\cdot\text{mol}^{-1}$, $n = 2.3$, and $\log A_D = -3.5$ (Ranalli, 1995).

Lastly, for the melts we have adopted the scheme proposed by Bittner and Schmeling (1995), in that the effective viscosity, η , of molten rocks ($M > 0.1$) is calculated from the following formula (Pinkerton and Stevenson, 1992):

$$\eta = \eta_0 \exp\{2.5 + [(1 - M)/M]^{0.48}(1 - M)\}, \quad (5)$$

where $\eta_0 = 10^{13} \text{ Pa s}$ ($\eta = 1 \times 10^{14} - 2 \times 10^{15} \text{ Pa s}$) is taken for the mafic rocks and $\eta_0 = 5 \times 10^{14} \text{ Pa s}$ ($\eta = 6 \times 10^{15} - 8 \times 10^{16} \text{ Pa s}$) is assumed for felsic metasedimentary rocks and granites (Bittner and Schmeling, 1995).

As the lower and upper cutoff values for viscosity of all types of rocks in our numerical experiments, we used 10^{17} and 10^{25} Pa s , respectively. This limitation implies that the viscosity of all molten rocks ($M > 0.1$) will be 10^{17} Pa s .

Mathematical Modeling and Numerical Implementation

We have considered two-dimensional creep flow, wherein both thermal and chemical buoyant forces are included. We have elected to employ the primitive variables of velocity, v , and pressure, P , in the momentum equation. The conservation of mass is approximated by the incompressible continuity equation

$$\partial v_x / \partial x + \partial v_z / \partial z = 0. \quad (6)$$

The two-dimensional Stokes equations with both thermal and chemical buoyancies take the form

$$\partial \sigma_{xx} / \partial x + \partial \sigma_{xz} / \partial z = \partial P / \partial x, \quad (7)$$

$$\partial \sigma_{zz} / \partial z + \partial \sigma_{xz} / \partial x = \partial P / \partial z - g \rho(P, T, C, M). \quad (8)$$

The density in the vertical component of the momentum equation depends explicitly on the temperature, T , the pressure, P , the composition, C , and the degree of melting, M . We do not explicitly consider the sub-grid process of percolation of melts (e.g., Scott and Stevenson, 1986), which would require a different set of governing equations (e.g., Connolly and Podladchikov, 1998; Vasilyev et al, 1998).

We employ viscous rheological constitutive relationships between the stress and strain-rate, whose coefficient η represents the effective creep viscosity $\eta(P, T, C, \dot{\epsilon}_{ij}, M)$, which

depends on the composition, temperature, pressure, strain-rate, and degree of melting

$$\begin{aligned} \sigma_{xx} &= 2\eta \dot{\epsilon}_{xx}, \\ \sigma_{xz} &= 2\eta \dot{\epsilon}_{xz}, \\ \sigma_{zz} &= 2\eta \dot{\epsilon}_{zz}, \\ \dot{\epsilon}_{xx} &= \partial v_x / \partial x, \\ \dot{\epsilon}_{xz} &= 1/2(\partial v_x / \partial z + \partial v_z / \partial x), \\ \dot{\epsilon}_{zz} &= \partial v_z / \partial z. \end{aligned}$$

The temperature equation takes the form

$$\rho C_p (\partial T / \partial t + v_x \partial T / \partial x + v_z \partial T / \partial z) = \partial q_x / \partial x + \partial q_z / \partial z + H_r, \quad (9)$$

$$\begin{aligned} q_x &= k \times (\partial T / \partial x), \\ q_z &= k \times (\partial T / \partial z), \\ H_r &= \text{constant}. \end{aligned}$$

The other notations used are x and z , respectively, for the horizontal and vertical coordinates in m; v_x and v_z for the components of the velocity vector, v , in $\text{m} \cdot \text{s}^{-1}$; t for the time in s; σ_{xx} , σ_{xz} , and σ_{zz} for the components of the viscous deviatoric stress tensor in Pa; $\dot{\epsilon}_{xx}$, $\dot{\epsilon}_{xz}$, and $\dot{\epsilon}_{zz}$ for the components of the strain-rate tensor in s^{-1} ; P for the pressure in Pa; T for the temperature in K; q_x and q_z , respectively, for the horizontal and vertical heat fluxes in $\text{W} \cdot \text{m}^{-2}$; η for the effective creep viscosity in Pa·s; ρ for the density in $\text{kg} \cdot \text{m}^{-3}$. $g = 9.81 \text{ m}\cdot\text{s}^{-2}$ is the gravitational acceleration; k is the thermal conductivity in $\text{W} \cdot \text{m}^{-1} \cdot \text{K}^{-1}$; C_p is the isobaric heat capacity in $\text{J} \cdot \text{kg}^{-1} \cdot \text{K}^{-1}$; H_r denotes radioactive heat production in $\text{W} \cdot \text{m}^{-3}$.

We have employed a recently developed thermomechanical two-dimensional code (I2) based on finite-differences with a marker technique that allows for the accurate conservative solution of the governing equations on a rectangular half-staggered Eulerian grid for multiphase viscous flow (Gerya et al., 2000). A detailed description of the numerical method and algorithmic tests is provided in Gerya et al. (2000).

RESULTS OF NUMERICAL EXPERIMENTS

Figure 4 illustrates relationships among material flow (left), temperature (middle), and viscosity (right) during reference model development. The early stages of the Rustenburg Layered Suite cooling process (0–0.5 m.y.) are characterized by massive outward-directed heat flow from the mafic intrusion, resulting in the generation and widening of zones of partially molten rocks with lowered viscosity in both overlying felsic volcanics and underlying sedimentary sequences. This is also associated with growth of the initial anticline in the intrusion floor, resulting in the formation of a dome composed of partially molten metasedimentary rocks. In contrast to common crustal dome structures (e.g., Bittner and Schmeling, 1995; Gerya et al., 2000), this dome is characterized by a 200–300 °C temperature increase from the core toward the margins. The next stages (0.5–0.8 m.y.) are manifested by rapid transformation of the dome into

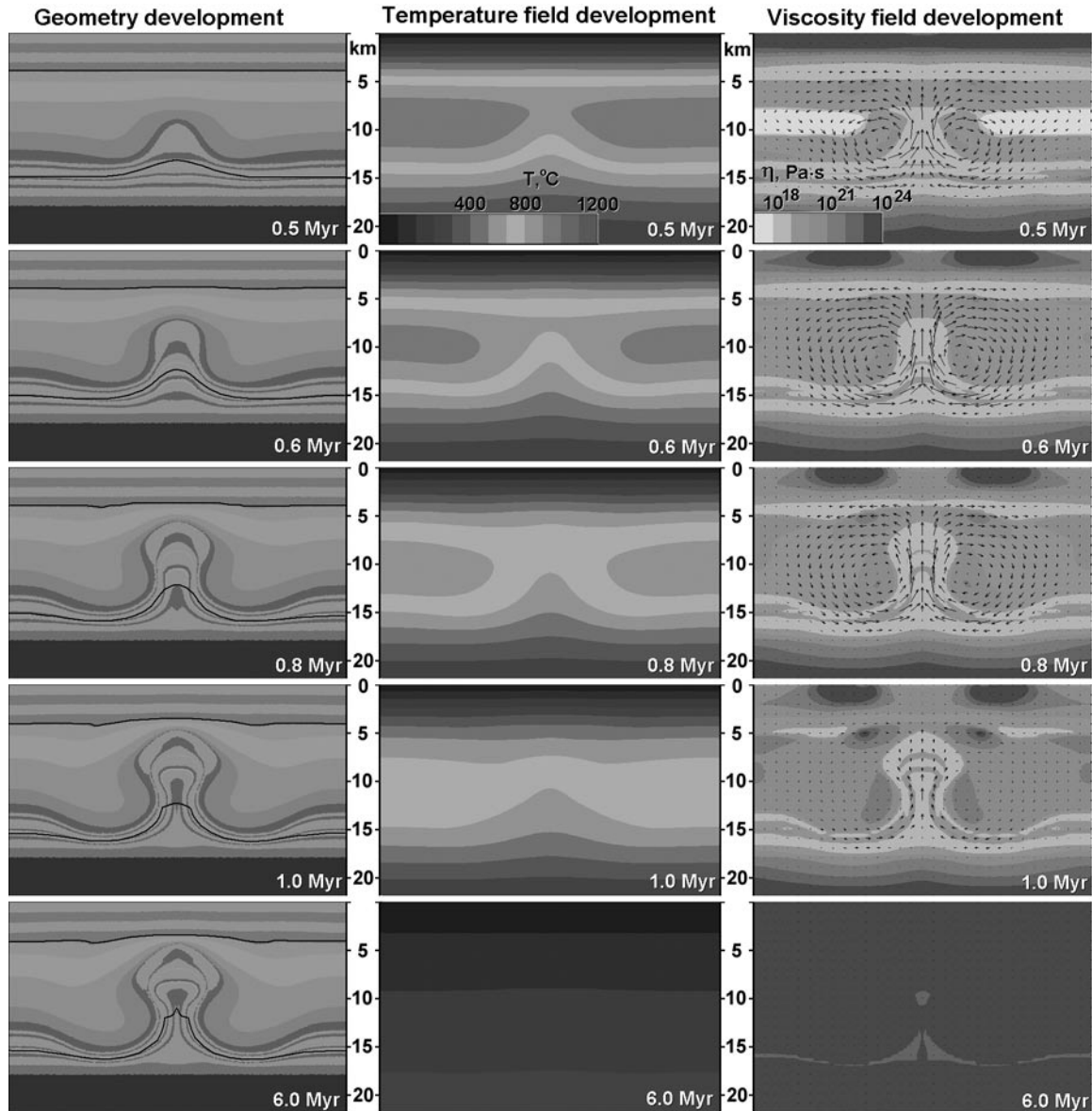


Figure 4. Results of numerical modeling showing the development of a diapir penetrating the magma chamber. The three columns represent calculated changes in geometry (left), thermal structure (middle), and viscosity (right) of the reference numerical model with time. Solid black line in the left column shows the maximum extent of migmatization in the felsic roof (upper line) and the sedimentary floor (lower line). Gray scale as in Figure 3. A color version of this figure is on the CD-ROM accompanying this volume.

an elongated diapir, with the characteristic 200–300 °C negative thermal anomaly, rapidly penetrating the Rustenburg Layered Suite intrusion and inducing cooling of the magmatic environment. This is also associated with the development of marginal synclines at the base of the diapir, accommodating thinning of the source sedimentary sequence (compare Figs. 2A and 4), and corresponding subsidence of mafic material. At the culminating stage of growth, the apical portion of the diapir penetrates the lower density, partially molten felsic roof sequence (compare

Figs. 1B and 4). Penetration of a diapir into lower density rocks is common when diapir growth is driven by gravitational instability at deeper crustal levels (Ramberg, 1981). Between 0.5 and 0.6 m.y., an inversion of the viscosity structure occurs. Initially, the viscosity of the partially molten felsic diapir is higher than that of the crystallizing mafic magma, but later, the diapir, although still partially molten, is characterized by a lower viscosity than the surrounding solidified mafic igneous rocks. The culminating stages of the cooling process (1.0–6.0 m.y.) are characterized by

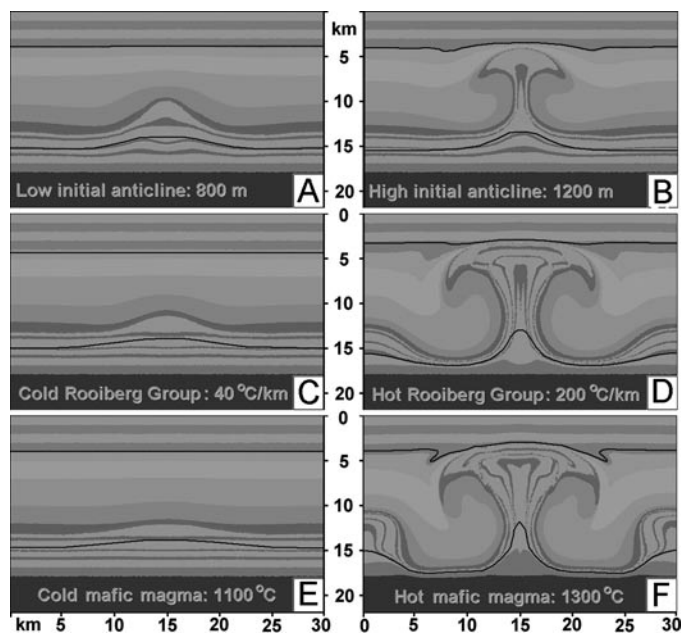


Figure 5. Changes in the final geometry of the diapir (cf. Fig. 4, bottom left) with changing initial conditions for diapir growth. A, B. Changes in the height of the initial anticline: A = 800 m; B = 1200 m. C, D. Changes in the initial temperature distribution within the Rooiberg Group: C = 25–225 °C ($\partial T/\partial z = 40$ °C/km); D = 25–1025 °C ($\partial T/\partial z = 200$ °C/km). E, F. Changes in the emplacement temperature of the Rustenburg Layered Suite: (E) = 1100 °C; F = 1300 °C. Other model parameters and gray scale as in Figure 3. A color version of this figure is on the CD-ROM accompanying this volume.

progressive cooling of the entire crustal sequence, resulting in a significant (several orders of magnitude) increase in viscosity of both the diapir and the surrounding rocks. This results in “freezing in” of the diapir geometry within the crystallizing mafic magmatic body. The average diapir growth rate before 1.0 m.y. is ~ 8 mm/y, consistent with previous estimates based on geological data (Uken and Watkeys, 1997).

Figures 5 and 6 illustrate the influence that changes in the model parameters (Table 2) have on the geometry and thermal structure of the diapir. Diapirism is dependent on the wavelength and, crucially, on the amplitude of the initial anticlinal disturbance. Diapirs are not developed when this amplitude is less than 800 m (Fig. 5A). The diapir geometry becomes inconsistent with field observations (exaggerated mushroom-like) when the amplitude is taken to be larger than 1000 m (Fig. 5B). Rapid growth of the diapir and its penetration (e.g., Fig. 4) into the roof of partially molten felsic volcanics of the Rooiberg Group and later Lebowa Granite Suite is consistent with field relations (Fig. 1B). Such penetration is controlled by the viscosity of the upper portion of the layered intrusion ~ 1 m.y. after the onset of the cooling process; only when this viscosity significantly exceeds that of the diapir does penetration into the roof not occur. The high temperatures and the presence of weak, partially crystallized mafic magma in the upper portion of the intrusion, which thus promotes this penetration, are presumably related to (1) the relatively high (~ 1200 °C) emplacement temperature of the ultramafic/mafic magma, (2) the crystallization differentiation process providing rapid heat exchange between upper and lower portions of the intrusion, and (3) prolonged (over 0.5–1 m.y.) addition of fresh hot mafic and/or felsic magmatic material into the top of the intrusion to compensate for cooling.

Variations in the initial temperature distribution within the model (Fig. 5C–F) also strongly affect diapir development and geometry: (1) the diapir fails to develop when there is a significant decrease in either the temperature gradient within the roof sequence (Fig. 5C) or the emplacement temperature of the Rustenburg Layered Suite (Fig. 5E), and (2) shows an unrealistic mushroom-like shape (Fig. 5D, F) complicated by additional domal structures when there is a significant increase in the above parameters. All these effects are mainly related to the exponential decrease in the effective viscosity of rocks

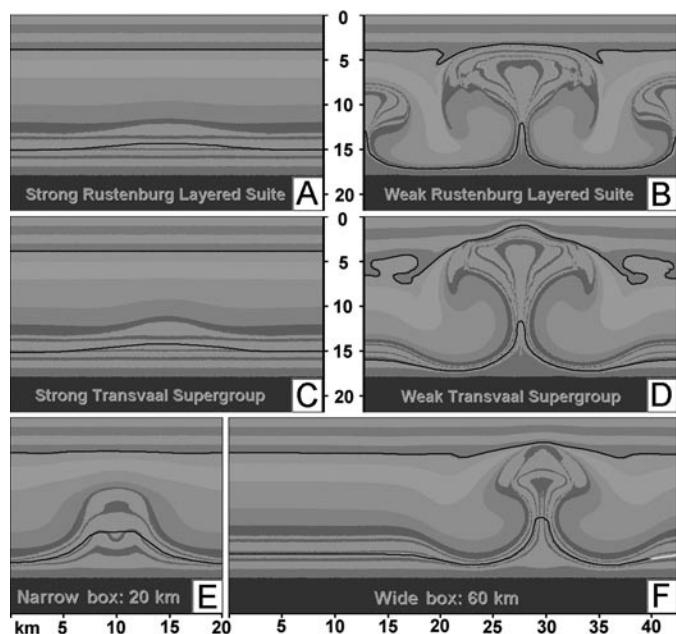


Figure 6. Changes in the final geometry of the diapir (cf. Fig. 4, bottom left) with changing rheology of rocks and size of the model. Strong/weak rheology is implemented by decreasing/increasing the A_D value in Equation 4 by a factor of 10. A, B. Changes in the rheology of the Rustenburg Layered Suite: A = strong rheology; B = weak rheology. C, D. Changes in the rheology of the Transvaal Supergroup: C = strong rheology; D = weak rheology. E, F. Changes in the lateral box size (initial wavelength): C = 20 km; D = 60 km (leftmost 43×22 km section of original 60×22 km symmetric model box is shown). Other model parameters and gray scale as in Figure 3. A color version of this figure is on the CD-ROM accompanying this volume.

with increasing temperature (Equation 4). Similar effects are obtained from changes in the rheological parameters used (Fig. 6A–D). We have varied the value of parameter A_D in Equation (4) by a factor of 10 to take into account possible variations in the effective rheology of the rocks (see Ranalli, 1995, and references therein). The diapirs are not developed when the rheology is significantly stronger (Fig. 6A, C) than in the reference model. Weaker rheology results in an unrealistic mushroom-like shape complicated by additional domal structures (Fig. 6B, D). The realistic (reference) geometry of the diapir (Fig. 4) could also be obtained by other combinations of the rheological parameters and the initial temperature distribution (e.g., by using both lowered emplacement temperature and weaker rheology of the Rustenburg Layered Suite). However, all geometrically realistic models are characterized by the same dynamics of diapiric ascent (Fig. 4), thus providing robust confirmation for the timing of the process as obtained in our numerical models.

A decrease in the characteristic lateral box size (i.e., in the characteristic size of the metasedimentary source area) results in a lower amplitude and more dome-like shape of the diapir (Fig. 6E). An increase in the size of the source area of up to 60 km (Fig. 6F) does not significantly affect the geometry and dynamics of ascent of the diapir, nor does it generate additional diapirs (cf. Fig. 6B) at the margins of the model. This further supports the suggestion that diapir nucleation was defined by the formation of initial anticline-shaped disturbances after fingered lateral injection of the Lower Zone of the Rustenburg Layered Suite between the felsic roof and sedimentary floor sequences (Uken and Watkeys, 1997). Due to this fingered emplacement, a variety of different anticlinal amplitudes and wavelengths were initially present, allowing preferential selection for diapiric growth during the cooling process.

CONCLUSIONS AND PERSPECTIVES

As follows from our two-dimensional numerical experiments, “cold” domes and diapirs represent an intriguing geological and thermomechanical feature of the Bushveld Complex. Such diapirs are related to the temporal inversion of a vertical temperature gradient due to the emplacement of large quantities of hot and heavy ultramafic and/or mafic magma onto a cold and less dense sedimentary succession (Johnson et al., 2003). Although this process has so far been described only from the Bushveld Complex, similar “cold” diapirism could have occurred in other mafic intrusions, provided they were large enough to furnish the necessary thermal energy and were endowed with the critical bottom topography indicated by our modeling (cf. Fig. 5). Moreover, similar thermomechanical phenomena may be expected in natural settings characterized by an inverted vertical temperature gradient (i.e., by a decrease in temperature with depth). Apart from well-known double-diffusive convection phenomena in magma chambers and salt fingers in the oceans (e.g., Hansen and Yuen, 1990), “cold,” partially molten diapirs have been shown to be common features in subduction zones (Tamura,

1994; Gerya and Yuen, 2003). Here, similar negative temperature anomalies are characteristic in association with the diapirs and plumes of hydrated, partially molten subducted and/or mantle material generated in the proximity of the upper interface of the subducting slab at a depth of >100 km (Davies and Stevenson, 1992; Tamura, 1994; Zhao et al., 2000, 2001; Gorbato et al., 1999; Tsumura et al., 2000; Hall and Kincaid, 2001; Tamura et al., 2002). According to both numerical (Davies and Stevenson, 1992; Gerya and Yuen, 2003) and analogue (Hall and Kincaid, 2001) modeling, these structures can rapidly penetrate the relatively hot asthenospheric portion of a mantle wedge. Positive buoyancy in the “cold” diapirs within the mantle wedge (Davies and Stevenson, 1992; Hall and Kincaid, 2001; Gerya and Yuen, 2003) is maintained by a compositional contrast and the presence of partially molten material in which melting is triggered by the fluid release from dehydration reactions within the subducting slab proceeding at depths of >100 km (Davies and Stevenson, 1992; Schmidt and Poli, 1998). The lower temperature of the diapirs (Tamura, 1994; Gerya and Yuen, 2003) with respect to the surrounding mantle wedge results from the inverted temperature gradient within the source region in proximity to the subducting slab (e.g., Davies and Stevenson, 1992; Gerya et al., 2002). The high diapiric uprise rate (Hall and Kincaid, 2001), which may exceed 10 cm/y (Gerya and Yuen, 2003), sustains this lower temperature. The diapiric features observed in the Bushveld Complex provide a unique opportunity to study “fossil evidence” of the “cold” diapir phenomenon and can lead to a broader recognition and understanding of this important geological process.

ACKNOWLEDGMENTS

The authors appreciate discussions with J. Van Decar concerning the general importance of the “cold diapir” phenomena. This work was supported by the University of Natal Research Fund, by the Russian Foundation of Basic Research grants 02-64405-64025, 03-05-64633, and 1645-2003-5, by the Swiss Federal Institute of Technology Research grant TH-12/04-1, by an Alexander von Humboldt Foundation Research Fellowship to T.V. Gerya, and by the Sonderforschungsbereich 526 at Ruhr-University, funded by the Deutsche Forschungsgemeinschaft. Constructive reviews by T. Johnson and an anonymous reviewer are greatly appreciated.

REFERENCES CITED

- Bittner, D., and Schmeling, H., 1995, Numerical modeling of melting processes and induced diapirism in the lower crust: *Geophysical Journal International*, v. 123, p. 59–70.
- Button, A., 1978, Diapiric structures in the Bushveld, north-eastern Transvaal: *Economic Geology Research Unit, University of the Witwatersrand Information Circular*, v. 123, p. 6.
- Cameron, E.N., 1978, The lower zone of the eastern Bushveld Complex in the Olifants River trough: *Journal of Petrology*, v. 19, p. 437–462.
- Cameron, E.N., 1980, Evolution of the lower critical zone, central sector, eastern Bushveld Complex, and its chromite deposits: *Economic Geology and the Bulletin of the Society of Economic Geologists*, v. 75, p. 845–871.

- Cameron, E.N., 1982, The upper critical zone of the Bushveld Complex, South Africa: *Economic Geology and the Bulletin of the Society of Economic Geologists*, v. 77, p. 1307–1327.
- Cawthorn, R.G., Cooper, G.R.J., and Webb, S.J., 1998, Connectivity between the western and the eastern limbs of the Bushveld Complex: *South African Journal of Geology*, v. 101, p. 291–298.
- Connolly, J.A.D., and Podladchikov, Yu.Yu., 1998, Compact-driven fluid flow in viscoelastic rock: *Geodinamica Acta (Paris)*, v. 11, p. 55–84, doi: 10.1016/S0985-3111(98)80006-5.
- Davies, H.J., and Stevenson, D.J., 1992, Physical model of source region of subduction zone volcanics: *Journal of Geophysical Research*, v. 97, p. 2037–2070.
- Du Plessis, A., and Kleywegt, R.J., 1987, A dipping sheet model for the mafic lobes of the Bushveld Complex: *South African Journal of Geology*, v. 90, p. 1–6.
- Eriksson, P.G., Schweitzer, J.K., Bosch, P.J.A., Schreiber, U.M., Van Devender, J.L., and Hatton, C.J., 1993, The Transvaal Sequence: an overview: *Journal of African Earth Sciences*, v. 16, p. 25–51, doi: 10.1016/0899-5362(93)90160-R.
- Gerya, T.V., and Yuen, D.A., 2003, Rayleigh-Taylor instabilities from hydration and melting propel "cold plumes" at subduction zones: *Earth and Planetary Science Letters*, v. 212, p. 47–62, doi: 10.1016/S0012-821X(03)00265-6.
- Gerya, T.V., Perchuk, L.L., Van Reenen, D.D., and Smit, C.A., 2000, Two-dimensional numerical modeling of pressure-temperature-time paths for the exhumation of some granulite facies terrains in the Precambrian: *Journal of Geodynamics*, v. 30, p. 17–35, doi: 10.1016/S0264-3707(99)00025-3.
- Gerya, T.V., Stoeckert, B., and Perchuk, A.L., 2002, Exhumation of high-pressure metamorphic rocks in a subduction channel—a numerical simulation: *Tectonics*, v. 21, p. 6-1–6-19, doi: 10.1029/2002TC001406.
- Gerya, T.V., Uken, R., Reinhardt, J., Watkeys, M.K., Maresch, W.V., and Brendan, C., 2003, Cold fingers in a hot magma: numerical modeling of country-rock diapirs in the Bushveld Complex, South Africa: *Geology*, v. 31, p. 753–756.
- Gorbatov, A., Dominguez, J., Suarez, G., Kostoglodov, V., Zhao, D., and Gordeev, E., 1999, Tomographic imaging of the P-wave velocity structure beneath the Kamchatka peninsula: *Geophysical Journal International*, v. 137, p. 269–279, doi: 10.1046/J.1365-246X.1999.00801.X.
- Hall, P.S., and Kincaid, C., 2001, Diapiric flow at subduction zones: A recipe for rapid transport: *Science*, v. 292, p. 2472–2475, doi: 10.1126/SCIENCE.1060488.
- Hansen, U., and Yuen, D.A., 1990, Nonlinear physics of double-diffusive convection in geological systems: *Earth-Science Reviews*, v. 29, p. 385–399, doi: 10.1016/0012-8252(90)90050-6.
- Harmer, R.E., and Armstrong, R.A., 2000, Duration of Bushveld Complex (sensu lato) magmatism: Constraints from new SHRIMP zircon chronology: Abstracts, Bushveld Complex Workshop, National Research Foundation, Gethlane Lodge, South Africa.
- Harris, N., McMillan, A., Holness, M., Uken, R., Watkeys, M., Rogers, N., and Fallick, A., 2003, Melt generation and fluid flow in the thermal aureole of the Bushveld Complex: *Journal of Petrology*, v. 44, p. 1031–1054, doi: 10.1093/PETROLOGY/44.6.1031.
- Hartzer, F.J., 1995, Transvaal Supergroup inliers: Geology, tectonic development and relationship with the Bushveld Complex, South Africa: *Journal of African Earth Sciences*, v. 21, p. 521–547, doi: 10.1016/0899-5362(95)00108-5.
- Hatton, C.J., and Schweitzer, J.K., 1995, Evidence for synchronous extrusive and intrusive Bushveld magmatism: *Journal of African Earth Sciences*, v. 21, p. 579–594, doi: 10.1016/0899-5362(95)00103-4.
- Johnson, T.E., Gibson, R.L., Brown, M., Buick, I.S., and Cartwright, I., 2003, Partial melting of metapelitic rocks beneath the Bushveld Complex, South Africa: *Journal of Petrology*, v. 44, p. 789–813, doi: 10.1093/PETROLOGY/44.5.789.
- Kaneko, Y., and Miyano, T., 1990, Contact metamorphism by the Bushveld Complex in the northeastern Transvaal, South Africa: *Journal of Mineralogy, Petrology and Economic Geology*, v. 85, p. 66–81.
- Marlow, A.G., and Van der Merwe, M.J., 1977, The geology and the potential economic significance of the Malope area, north-eastern Bushveld Complex: *Transactions of the Geological Society South Africa*, v. 80, p. 117–123.
- Molyneux, T.G., and Klinkert, P.S., 1978, A structural interpretation of part of the eastern mafic lobe of the Bushveld Complex and its surroundings: *Transactions of the Geological Society South Africa*, v. 81, p. 359–368.
- Pinkerton, H., and Stevenson, R.J., 1992, Methods of determining the rheological properties of magmas at subliquidus temperatures: *Journal of Volcanology and Geothermal Research*, v. 53, p. 47–66, doi: 10.1016/0377-0273(92)90073-M.
- Ramberg, H., 1981, Gravity, deformation and geological application: London, New York, San Francisco, Academic Press, 452 p.
- Ranalli, G., 1995, Rheology of the Earth, 2nd edition: London, Chapman and Hall, 413 p.
- Scott, D.R., and Stevenson, D.J., 1986, Magma ascent by porous flow: *Journal of Geophysical Research*, v. 91, p. 9283–9296.
- Sharpe, M.R., 1986, Eastern Bushveld Complex Excursion Guidebook: Extended Abstracts, Geocongress '86, Geological Society of South Africa, Johannesburg, p. 135.
- Sharpe, M.R., and Chadwick, B., 1982, The geometry of floor folds and xenoliths in the eastern compartment of the Bushveld Complex: *Transactions of the Geological Society of South Africa*, v. 85, p. 29–42.
- Sharpe, M.R., and Snyman, J.A., 1980, A model for the emplacement of the eastern compartment of the Bushveld Complex: *Tectonophysics*, v. 65, p. 85–110, doi: 10.1016/0040-1951(80)90225-5.
- Schmidt, M.W., and Poli, S., 1998, Experimentally based water budgets for dehydrating slabs and consequences for arc magma generation: *Earth and Planetary Science Letters*, v. 163, p. 361–379, doi: 10.1016/S0012-821X(98)00142-3.
- Tamura, Y., 1994, Genesis of island arc magmas by mantle-derived bimodal magmatism: evidence from the Shirahama Group, Japan: *Journal of Petrology*, v. 35, p. 619–645.
- Tamura, Y., Tatsumi, Y., Zhao, D.P., Kido, Y., and Shukuno, H., 2002, Hot fingers in the mantle wedge: new insights into magma genesis in subduction zones: *Earth and Planetary Science Letters*, v. 197, p. 105–116, doi: 10.1016/S0012-821X(02)00465-X.
- Tsumura, N., Matsumoto, S., Horiuchi, S., and Hasegawa, A., 2000, Three-dimensional attenuation structure beneath the northeastern Japan arc estimated from spectra of small earthquakes: *Tectonophysics*, v. 319, p. 241–260, doi: 10.1016/S0040-1951(99)00297-8.
- Turcotte, D.L., and Schubert, G., 1973, Frictional heating of the descending lithosphere: *Journal of Geophysical Research*, v. 78, p. 5876–5886.
- Turcotte, D.L., and Schubert, G., 1982, *Geodynamics: application of continuum physics to geological problems*: New York, John Wiley, 450 p.
- Uken, R., 1998, The Geology and Structure of the Bushveld Complex metamorphic aureole in the Olifants River area [Ph.D. thesis]: Durban, South Africa, University of Natal, 277 p.
- Uken, R., and Watkeys, M.K., 1997, Diapirism initiated by the Bushveld Complex, South Africa: *Geology*, v. 25, p. 723–726, doi: 10.1130/0091-7613(1997)0252.3.CO;2.
- Vasilyev, O.V., Podladchikov, Y.Y., and Yuen, D.A., 1998, Modeling of compaction driven flow in poro-viscoelastic medium using adaptive wavelet collocation method: *Geophysical Research Letters*, v. 25, p. 3239–3243, doi: 10.1029/98GL52358.
- Von Gruenewaldt, G., Sharpe, M.R., and Hatton, C.J., 1985, The Bushveld Complex: Introduction and review: *Economic Geology and the Bulletin of the Society of Economic Geologists*, v. 80, p. 803–812.
- Walraven, F., Armstrong, R.A., and Kruger, F.J., 1990, A chronostratigraphic framework for the north-central Kaapvaal craton, the Bushveld Complex and the Vredefort structure: *Tectonophysics*, v. 171, p. 23–48, doi: 10.1016/0040-1951(90)90088-P.
- Waters, D.J., and Lovegrove, D.P., 2002, Assessing the extent of disequilibrium and overstepping of prograde metamorphic reactions in metapelites from the Bushveld Complex aureole, South Africa: *Journal of Metamorphic Geology*, v. 20, p. 135–149, doi: 10.1046/J.0263-4929.2001.00350.X.
- Zhao, D.P., Asamori, K., and Iwamori, H., 2000, Seismic structure and magmatism of the young Kyushu subduction zone: *Geophysical Research Letters*, v. 27, p. 2057–2060, doi: 10.1029/2000GL011512.
- Zhao, D.P., Wang, K.L., Rogers, G.C., and Peacock, S.M., 2001, Tomographic image of low P velocity anomalies above slab in northern Cascadia subduction zone: *Earth Planets and Space*, v. 53, p. 285–293.

